

# Testing the ‘clump’ model of SiO maser emission

M. D. Gray<sup>1</sup>, R. J. Ivison<sup>2</sup>, E. M. L. Humphreys<sup>1,3</sup> and J. A. Yates<sup>4</sup>

<sup>1</sup> *Department of Physics, University of Bristol, Tyndall Avenue, Bristol BS8 1TL*

<sup>2</sup> *Institute for Astronomy, University of Edinburgh, Royal Observatory, Blackford Hill, Edinburgh EH9 3HJ*

<sup>3</sup> *School of Chemistry, University of Bristol, Cantock’s Close, Bristol BS8 1TS*

<sup>4</sup> *Department of Physical Sciences, University of Hertfordshire, College Lane, Hatfield AL10 9AB*

Accepted ... . Received ... ; in original form ...

## ABSTRACT

Building on the detection of the  $J = 7-6$  SiO maser emission in both the  $v = 1$  and  $v = 2$  vibrational states towards the symbiotic Mira, R Aquarii, we have used the James Clerk Maxwell Telescope to study the changes in the SiO maser features from R Aqr over a stellar pulsational period. The observations, complemented by contemporaneous data taken at 86 GHz, represent a test of the popular thermal-instability clump models of SiO masers. The ‘clump’ model of SiO maser emission considers the SiO masers to be discrete emitting regions which differ from their surroundings in the values of one or more physical variables (SiO abundance for example). We find that our observational data are consistent with a clump model in which the appearance of maser emission in the  $J = 7-6$  transitions coincides with an outward-moving shock impinging on the inner edge of the maser zone.

**Key words:** masers — binaries: symbiotic — stars: individual: R Aqr — radio lines: stars

## 1 INTRODUCTION

R Aqr is a well-known symbiotic Mira, exceptional in that its envelope supports maser emission (Martinez et al. 1988; Schwarz et al. 1995). SiO maser emission has been detected in the low rotational excitation transitions  $J = 2-1$  and  $J = 1-0$ , and R Aqr is also one of only two symbiotic Miras to exhibit H<sub>2</sub>O masers (22 GHz: Ivison, Seaquist & Hall 1994, 1995; 321 GHz: Ivison, Yates & Hall 1998).

SiO maser emission in the  $J = 7-6$  rotational transitions of vibrational states  $v = 1$  and  $v = 2$  had been predicted by theoretical models (Doel et al. 1995; Gray et al. 1995) and, although observations towards some of the brightest nearby masing objects failed to detect these lines, they were detected towards R Aqr (Gray et al. 1996). Following this initial discovery,  $J = 7-6$  SiO masers have been detected towards several stars of Mira, semi-regular variable and supergiant types, proving that emission in these lines is not based on the symbiotic nature of R Aqr (Humphreys et al. 1997a).

The objective was to study the variation of the SiO maser spectra, in both of the 300-GHz lines detected to date, over a stellar pulsational period. This sequence of observations makes it possible to investigate the validity of the ‘clump’ model of SiO maser emission, which considers the SiO masers to be discrete emitting regions which differ from their surroundings in the values of one or more physical variables (SiO abundance, for example). Positional consid-

erations dictate that data for some stellar phases will be unobtainable with observations made during a single stellar period (over several stellar periods, in fact, because the period of R Aqr is close to 1 yr) but the nature of variability in SiO masers meant that it would be unwise to augment the incomplete phase data with material drawn from the same phase in subsequent periods.

Observational support for discrete SiO emitting regions has come from recent VLBI studies of SiO masers at 43 GHz (Diamond et al. 1994; Miyoshi et al. 1994; Greenhill et al. 1995), where rings of maser emission are resolved into individual maser features on the milli-arcsecond scale. The spectra we observe are therefore a superposition of the individual line shapes of many discrete objects, in the same way that the molecular line profile of a galaxy is the result of emission from many discrete molecular clouds. Very recent VLBI observations of SiO masers (Boboltz et al. 1997) in the circumstellar envelope of R Aqr at 43 GHz, using the VLBA, show that the masers form a ring structure, similar to those found in other Mira variables. Moreover, Boboltz et al. show convincingly that the ring of 43-GHz masers around R Aqr was contracting at an average speed of  $4 \text{ km s}^{-1}$  between 1995 December 29 and 1996 April 05. By coincidence, this time period overlaps with some of the observing epochs used in the present work.

It is well known that SiO maser fluxes in the lower rotational transitions vary considerably, both within the stellar period and between different periods, in several SiO maser

arXiv:astro-ph/9712124v1 8 Dec 1997

sources. R Aqr is no exception; variation in the  $v = 1$ ,  $J = 2 - 1$  transition is clearly shown by Schwarz et al. (1995) and in the  $v = 1$ ,  $J = 2 - 1$  spectra in Fig. 1 of the present work.

In the ‘clump’ model, the variability of the SiO maser spectra is interpreted as resulting primarily from the motion of the maser regions as they follow the pulsations of the stellar envelope. As the masing objects move, they experience changes in the radiation fields incident upon them and may change in density and temperature. These changes in physical conditions cause fluctuations in the maser emission, which may be observed as a change in flux, or in the line profile(s) which a particular object emits. An abrupt change in the physical conditions will occur once per cycle due to passage through an outward-moving shock front.

From our computational models (Humphreys et al. 1996; Humphreys et al. 1997b), the number of spots which contribute significantly to a SiO maser spectrum falls with increasing rotational excitation. On this basis, we would expect clumps emitting in  $J = 7 - 6$  lines to be much rarer than those emitting in, say, the  $J = 2 - 1$  lines. Our prediction regarding the  $J = 7 - 6$  lines would therefore be of an almost catastrophic form of variability, since the loss of two or three dominant clumps could eradicate the entire spectrum in these transitions and the emission could remain absent for some considerable fraction of the stellar period. The loss of a similar number of clumps would be likely to produce a more subtle change in the  $J = 1 - 0$  or  $J = 2 - 1$  masers, which appear to be composed of several tens of emitting clumps in most Miras (for example, Diamond et al. 1994). R Aqr appears to have a fairly typical number of 43-GHz SiO maser spots (Boboltz et al. 1997).

A plausible mechanism for the formation of SiO maser clumps is through thermal instabilities resulting from infrared band cooling by CO and SiO (Cuntz & Muchmore 1994). Thermal instabilities of this type result in a bifurcated envelope structure with two phases which differ in kinetic temperature (by typically 200–300 K) and in molecular abundance. One phase would form the maser clumps and the other a hotter background medium.

The observations described here enable us to test this theory of the origin of SiO maser clumps by measuring the lifetimes of maser features in the observed spectra against the timescales predicted by Cuntz & Muchmore (1994). The  $J = 7 - 6$  lines are particularly valuable for this task, since they are likely to arise from the contributions of only a few emitting clumps (as discussed earlier). New spectral features should appear on the cooling timescale ( $< 10^6$  s) and should last until a clump is re-heated by the passage of a shock-wave. Shocks would be likely to modify each clump approximately once per pulsational period, or on a timescale of  $\sim 3.3 \times 10^7$  s, in the particular case of R Aqr, which is much larger than the cooling time.

## 2 OBSERVATIONS

The 15-m James Clerk Maxwell Telescope (JCMT), Mauna Kea, Hawaii, was used over a period of one year to monitor the  $J = 7 - 6$  SiO lines ( $v = 1$  and  $v = 2$ ) towards R Aqr. The rest frequencies used were 301.814 GHz for the  $v = 1$  transition and 299.704 GHz for the  $v = 2$  transition, with a veloc-

**Table 1.** High-frequency SiO maser data from the JCMT.

UT Date	Line Frequency	Peak Flux
	/GHz	/Jy
1995 Jun 08	299	9.7
	301	26
1996 Feb 27	299	5.4
	301	4.4
1996 Mar 15	299	7.6
	301	5.9
1996 Jun 28	299	9.5
	301	4.7
1996 Jul 27 <sup>†</sup>	299	7.9
	301	4.8
1996 Sep 15	301	<3.0
1996 Oct 06	301	<1.0
1996 Oct 22	299	<3.6
1996 Dec 01	299	1.7
	301	<1.9

<sup>†</sup> indicates an average, at 299 GHz, of two close epochs (1996 July 27 and 29).

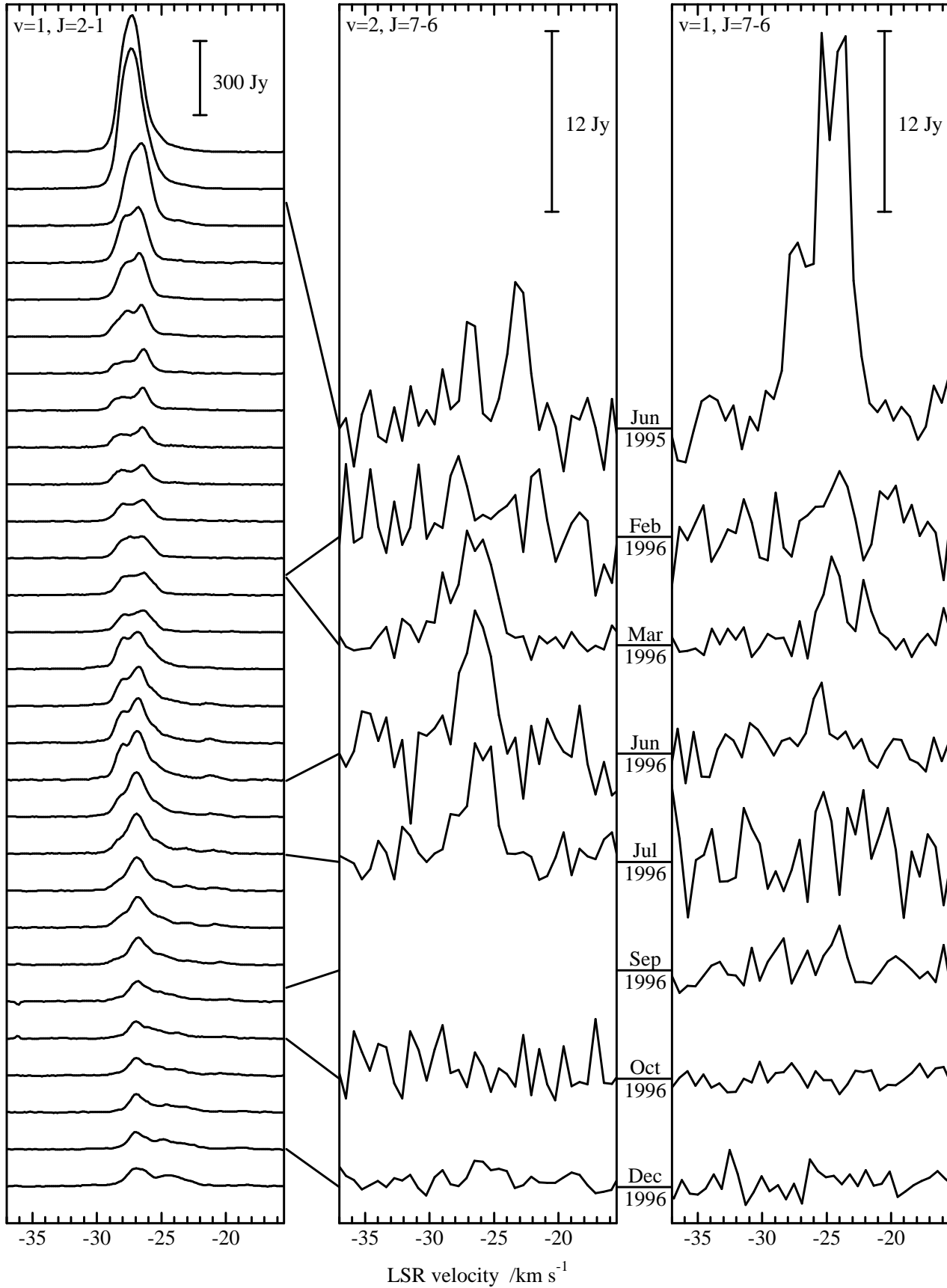
ity of  $-25.0 \text{ km s}^{-1}$  relative to the LSR. The liquid-helium-cooled, single-channel SIS mixer receiver B3i was used, with a digital autocorrelation spectrometer backend providing a bandwidth of 250 MHz with channel spacings of 0.125 MHz (later binned to 0.625 MHz or  $0.63 \text{ km s}^{-1}$ ). The  $v = 1$  and  $v = 2$  lines were tuned in the upper and lower sidebands, respectively. The time spent on source (inclusive of overheads for sky subtraction, exclusive of other overheads, such as the time spent nodding the telescope to alternate the signal and reference beams) varied between 1200 and 5400 s. Values of  $T_{\text{rec}}$  were around 200 K, whilst  $T_{\text{sys}}$  varied between 500 and 1400 K. JCMT data are summarised in Table 1.

R Aqr, supporting a very bright SiO maser at 86.243 GHz, is regularly used as a pointing source at the 15-m Swedish-ESO Submillimetre Telescope (SEST), La Silla, Chile. Data from short integrations (300 s, typically) taken during the period between 1995 June and 1996 December using the dual-polarization Schottky receiver and the acousto-optical high-resolution spectrometer (43-kHz channel spacings) were kindly made available to us (L.-Å. Nyman, private communication). SEST data are summarised in Table 2.

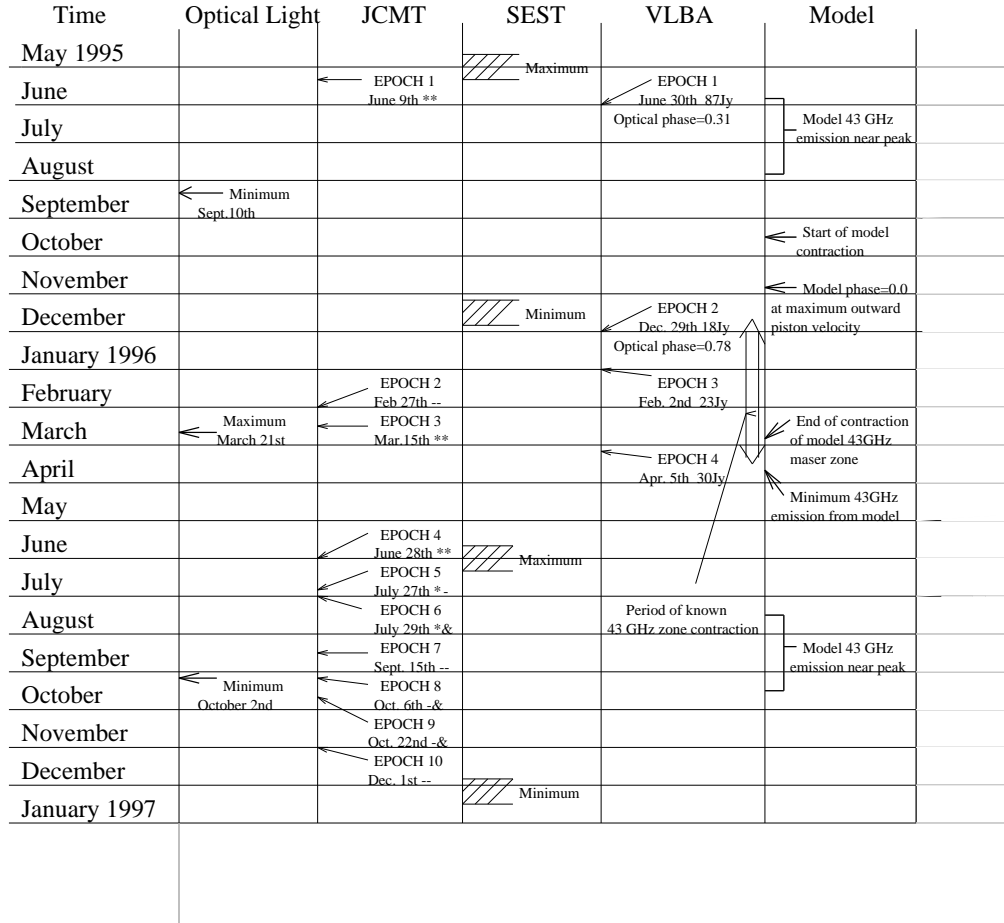
## 3 RESULTS AND DISCUSSION

Fig. 1 shows the observed spectra of the SiO  $J = 2 - 1$  and  $J = 7 - 6$  lines towards R Aqr. These data were reduced in the standard manner, using SPECX V6.7 (Padman 1993). Data reduction included re-binning to produce channels of width  $0.63 \text{ km s}^{-1}$  (from five observational bins in the case of the  $J = 7 - 6$  lines). Conversion from the  $T_{\text{A}}^*$  scale to flux-density units was achieved using a conversion factor of  $30 \text{ Jy K}^{-1}$  for the data from the JCMT and  $25 \text{ Jy K}^{-1}$  for data from SEST.

Inspection of Fig. 1 shows that all the SiO maser lines observed are highly variable over time, as expected. A comparison of the  $J = 2 - 1$  and  $J = 7 - 6$  spectra shows that the  $J = 7 - 6$  spectra are probably more variable than the  $J = 2 - 1$  spectra. However the comparatively low number of epochs available for the high-frequency observations reduces the significance of this conclusion. It is also clear that whilst the  $J = 2 - 1$  transition shows considerable variation



**Figure 1.** R Aqr SiO maser transitions obtained during the course of 1995–96 (top to bottom). Left:  $v = 1, J = 2 - 1$  maser (86 GHz); centre:  $v = 2, J = 7 - 6$  maser (299 GHz); right:  $v = 1, J = 7 - 6$  maser (301 GHz). Lines between the panels indicate data that are contemporaneous.



**Figure 2.** Timeline for the observations discussed in this work together with model data used in their interpretation. Symbols following the epoch date in the JCMT column have the following meanings: \* observed and detected; - observed and not detected; & no observation. The first symbol relates to 299 GHz and the second to 301 GHz in each case.

in intensity over the duration of the experiment (a factor of 8.33 in peak intensity between the brightest and weakest epochs), the  $J = 2 - 1$  maser never disappears entirely. On the contrary, the  $\nu = 1$ ,  $J = 7 - 6$  line appears to be entirely absent, to a  $3-\sigma$  level of  $< 1$  Jy during 1996 October, a factor of at least 25 lower than the largest peak in this transition. The  $\nu = 2$ ,  $J = 7 - 6$  line is probably also absent for part of the experimental period, but higher noise makes this less statistically significant.

The shape of the high-frequency spectra for both lines is highly variable. It is clear from Fig. 1 that the line profiles have changed significantly between 1996 March 15 and June 28 and again between the latter date and July 27. Only over the shortest timescale, two days between 1996 July 27 and 29, was the 299-GHz line profile very similar and these two spectra have been averaged in Fig. 1. There was no 301-GHz observation on July 29. This variability suggests that

the clumps supporting high-frequency masers have lifetimes of between 2 and 30 d.

R Aqr has a pulsational period of 387 d. From the AAVSO phase data in Boboltz et al. (1997), the period covered by our data contains two optical minima and one maximum. From these same phase data, we can fix the optical maximum to 1996 March 21 to an accuracy of 1 d. We note that the light curve of R Aqr is slightly skewed, with the rise from minimum to maximum taking only 0.42 of a cycle (Kholopov, 1985). This information allows us to fix the minima, which are less well defined than maxima in R Aqr, to 1995 October 11 and 1996 November 02. The minima, however, are not used as timing markers for synchronization with other data and are much less important than the maxima in the present work. We also know that the envelope region containing the 43-GHz masers was shrinking between late 1995 December and early 1996 April. A likely sequence of events can be constructed from a combination of

**Table 2.** SiO maser data from SEST.

UT Date	Peak Flux /Jy	Integrated Flux /Jy km s <sup>-1</sup>
1995 May 25	553	1300
1995 Jun 02	570	1400
1995 Jul 07	335	830
1995 Aug 13	226	580
1995 Aug 25	189	470
1995 Sep 21	128	340
1995 Oct 24	98.9	240
1995 Oct 30	92.6	240
1995 Nov 07	82.6	220
1995 Nov 15	78.9	230
1995 Dec 02	86.9	260
1995 Dec 15	89.1	290
1996 Jan 04	91.9	290
1996 Jan 18	88.0	270
1996 May 01	151	480
1996 May 23	159	470
1996 Jun 10	181	540
1996 Jun 28	198	590
1996 Jul 13	181	510
1996 Jul 30	163	470
1996 Aug 07	136	380
1996 Aug 21	124	380
1996 Sep 06	109	320
1996 Sep 21	82.1	300
1996 Oct 07	69.8	220
1996 Oct 16	71.1	220
1996 Nov 22	74.6	230
1996 Dec 05	69.2	250
1996 Dec 27	73.3	300

our data, the work of Boboltz et al. and the hydrodynamic models of Bowen (1988, 1989) augmented by maser models as in Humphreys et al. (1996). The behaviour of these various aspects of the envelope are summarized in the composite timeline shown in Fig. 2.

Both the 300-GHz lines were probably present on 1996 February 27, but detections were marginal because of high noise levels. Both masers were detected on 1996 March 15. These same masers were then detected on three more occasions in 1996 June and July (a 301-GHz observation was not attempted on the last of these occasions). These were the final strong detections: further observations in 1996 September, October (2 sets) and December failed to detect either line, except for a marginal detection (1.7 Jy) of the 299-GHz line in 1996 December. It is unfortunate that additional data could not be taken in 1996 April or May, but it appears to be the case that 300-GHz masers were active much of the time between 1996 March and the end of 1996 July. These were then destroyed, by passage through a shock or by some other adjustment to prevailing physical conditions unsuitable for  $J = 7 - 6$  emission, at some time in 1996 August or early September and never re-formed during the remainder of the experiment.

If we now consider the hydrodynamic situation, the zero model phase (maximum expansion velocity of the sub-surface ‘piston’ into the photosphere) occurs at visual phase  $\sim 0.7$  (Humphreys et al. 1996), which in this case would be either in late 1995 November, or just after the final set of JCMT observations in mid-1996 December. The period for which the model 43-GHz maser zone is in contraction lasts

from model phase  $\sim 0.85 - 0.90$  to model phase  $\sim 0.25 - 0.35$ . Masing clumps with larger than average radial positions tend to contract, in modelling results, until the larger phase value and vice-versa (Humphreys et al. 1997b). It can be seen from Fig. 2 that the model and observed contraction zones are compatible to within  $\sim 0.05$  of a complete cycle (17 d) provided that the observations performed by Boboltz et al. represent the latter stages of the 43-GHz zone contraction. If this synchronization of the model and the VLBA data is adopted, a consequence is that a small phase-lag of 0.1 – 0.2 of a period should appear between the SEST (86-GHz) data and the VLBA (43-GHz) data. Unfortunately there are only four VLBA epochs, so this prediction cannot be tested exactly, but the 87-Jy VLBA signal shortly after the first SEST maximum in Fig. 2, compared to the much lower fluxes measured during the contraction period (18–30 Jy) indicate that the data are not inconsistent with a small phase difference between the 43- and 86-GHz cycles, with the 43-GHz cycle leading. The position of the cycle minimum in the model output is considerably less well defined than the maximum and could occur somewhat earlier, but not later than its marked position in Fig. 2.

Turning now to the 300-GHz data, there appears to be a significant phase-lag between the  $J = 7 - 6$  maser emission and both the low-frequency lines, assuming a 300-GHz peak somewhere between mid-March 1996 and late Jun 1996 (model phase between  $\sim 0.35$  and  $\sim 0.65$ ). In fact, the lag with respect to the 43-GHz emission would amount to almost half a cycle. The large phase lag of the 300-GHz masers with respect to those at low frequency means that the data are not consistent with the idea that objects masing at 300 GHz are destroyed by the passage of a shock wave through the maser zone: instead, they must be rapidly created in its aftermath and die away for an entirely different reason. Passage of the shock through the 43-GHz maser zone can be timed observationally, to early April at the earliest, since it would end the episode of infall. However, data from Boboltz et al. represent a broad average over many maser features and the model data show that individual spots should be struck by the shock as early as late February or as late as late April, depending on the mean radial position of the spot: spots with smaller mean radial positions suffering impact by the shock at earlier times. The 300-GHz masers become strong between 1996 February 27 and March 15. If the clumps which give rise to this high-frequency emission are those which lie, on average, closest to the star, then they could be produced by shock impact in late February or early March, followed by a period of cooling to below 4500 K when thermal instabilities allow the formation of clumps. It is noted that model predictions are that the vast majority of  $J = 7 - 6$  emission is produced by clumps with temperatures between 3000 and 5000 K, consistent with clumps formed by the action of the higher density regions of Cuntz & Muchmore’s ‘CO Instability Island’ for a stellar temperature of 3000 K.

### 3.1 Timescales

Three timescales are important in determining the behaviour of the post-shock material: the hydrodynamic time,  $\tau_H$ , the radiative cooling time,  $\tau_R$  and the chemical time  $\tau_C$ . The hydrodynamic time is the timescale on which the

post-shock gas will cool if there is negligible radiative cooling. In the inner regions of a Mira envelope, where overall expansion is a small perturbation on the shock-wave and gravity driven cyclic motions, the formula for  $\tau_{\text{H}}$  in Cuntz & Muchmore (1994) reduces to  $\tau_{\text{H}}=c_{\text{m}}P/2u_2$  where  $P$  is the stellar pulsational period,  $c_{\text{m}}$  is the average sound speed in the envelope at a given radius and  $u_2$  is the velocity of the post-shock gas. The speed,  $c_{\text{m}}$ , is a weak function of radius and a mean value of  $3.4 \text{ km s}^{-1}$  has been used for the whole maser zone.

The radiative cooling time is the timescale on which the post-shock gas will cool back to the local radiative equilibrium temperature, provided that the most efficient coolant species, for a given temperature and composition, are present in the gas. The presence of the coolant species depends on the chemical time. Cooling times given in Cuntz & Muchmore (1994), based on CO cooling, with a small contribution from SiO, agree well with those predicted by the more sophisticated cooling function developed in Woitke et al. (1996). The good agreement relies on the fact that the total cooling time is dominated by the slowest phase, between about 7000 K and the instability temperatures of 4000–4500 K which is also dominated by CO infrared band cooling. We note that if efficient radiative cooling applies, the shocks will be closer to isothermality than those in the Bowen models, with the result that the enhanced temperature regions behind the shocks would be markedly thinner than those which appear in, for example, Fig. 1a of Humphreys et al. (1996).

The chemical time is the most difficult of the three timescales to evaluate because it depends on a complex reaction network: it is the longest of a set of timescales, each of which is a typical time taken to re-establish the equilibrium abundance of an important species. In the present work, the important species are CO (for cooling), SiO (for masing and cooling) and  $\text{H}_2$  (because the collisional rate coefficients used in the maser modelling are a better representation of collisions between SiO and  $\text{H}_2$  than between SiO and H). Chemical timescales are not calculated in any detail in Cuntz & Muchmore and we have adopted the more accurate values calculated in Beck et al. (1992). We have used the standard Model A from Beck et al. with the modified temperature structure from Wirsich (1988). High-temperature post-shock regions mean that there is sufficient radiation to drive some photochemistry, making Model A the better approximation to our system for most parameters, whilst the temperature structure from Wirsich is a better approximation to the Bowen data than the monotonic decay from 1100 K at  $2R_*$  used in the standard Model A. The timescale for CO is the longest at all radii of interest, so this is taken as the chemical time. All three timescales are tabulated for post-shock conditions in Table 3.

It can be seen from Table 3 that the chemical timescale is the shortest of the three timescales at all radii, so we expect that the necessary coolant and masing molecules will be regenerated following the passage of a shock before significant cooling occurs by expansion. Cooling should therefore occur on the radiative timescale because it is, firstly, markedly shorter than the timescale for hydrodynamic cooling, and secondly, considerably longer than the chemical time required to reform the coolant molecules dissociated by the passage of the shock. This latter condition renders

**Table 3.** Conditions in the post-shock gas as a function of model phase,  $\phi$ .

$\phi$	$R_{\text{S}}/R_*$	$\tau_{\text{H}}/d$	$\tau_{\text{R}}/d$	$\tau_{\text{C}}/d$	$n_2/\text{cm}^{-3}$	$n_2/n_1$
0.0	1.25	67	0.17	0.005	7.9(12)	140
0.25	1.83	80	0.59	0.012	7.1(10)	28
0.5	2.40	99	0.97	0.058	1.0(10)	13
0.75	2.80	95	1.50	0.183	2.5(9)	11

Note: The bracket notation has the mantissa outside the bracket and the decimal exponent inside so, for example,  $7.9(12) = 7.9 \times 10^{12}$ .  $R_{\text{S}}$  is the radial position of the shock front,  $n_1$  is the pre-shock density and  $n_2$  the post-shock density after the gas has cooled to 4500 K. Initial post-shock temperatures lie between 8000 and 10000 K for all phases in the table.

it unnecessary to include a contribution for the chemistry in the cooling time. A significant delay appears between the model phase zero and the appearance of the first 300-GHz masers. This is almost certainly because the density of the post-shock material (see Table 3) is too high to allow the necessary population inversions to develop before a phase of about 0.25. Once the post-shock conditions are suitable, maser clumps can develop via cooling instabilities on a timescale of 1–2 d. The 300-GHz masers would be the youngest masing objects, forming at the highest instability temperatures of around 4000–4500 K (Cuntz & Muchmore 1994). The lifetimes of 300-GHz maser clumps would be governed by a period of slower cooling towards the inter-shock temperature of the envelope ( $\sim 1500$  K) on a timescale of 5–20 d, consistent with the variability of the high-frequency spectra (Fig. 1).

Further evolution of the circumstellar shell probably follows the sequence described here: the original 300-GHz emitting clumps cool further and begin emitting instead in lower frequency lines, whilst as the shock progresses outwards through the envelope it destroys existing low-frequency emitting clumps and generates new high-frequency emitters. Eventually, beyond a model phase of about 0.70–0.75, the shock becomes too weak to generate new clumps that emit at 300 GHz: the crucial factor here is probably the post-shock density, which becomes too low. As existing clumps cool below  $\sim 3000$  K, the  $J = 7 - 6$  masers disappear. We know from observations that most of the  $J = 7 - 6$  masers were lost between early August and mid-September 1996 at a model phase of between 0.68 and 0.77. Model predictions (Humphreys et al. 1997b) suggest that for model phases  $> 0.7$ – $0.75$ , the 43- and 86-GHz maser shells in  $v = 1$  should be similar in size, with the 86-GHz shell being slightly the larger and less well defined. Over a similar phase range, the peak amplifications in the synthetic maser are in the ratio of  $\sim 2:1$  in favour of the 43-GHz transition.

The original detection of the 300-GHz lines clearly belongs to an earlier pulsational cycle than the rest of the data. These data were taken nearly four months before the optical minimum of 1995 October 2 and should therefore correspond roughly to the 1996 June or July observations. The fact that the 300-GHz lines were much brighter than features detected one period later is further evidence for the variability of SiO emission between phases, already well established at 43 and 86 GHz (Nyman & Oloffson 1986; Martinez et al. 1988). Evidently the earlier pulsational cycle was also better suited

to 86-GHz emission, as seen in the relative intensities of the peaks near the beginning of 1996 October and the earliest SEST data (which is much brighter, although almost certainly past the peak of the previous pulsation). It is not clear from this work why any one cycle should favour SiO maser emission, at any frequency, over any other cycle.

#### 4 CONCLUDING REMARKS

In this paper we report monitoring observations of SiO maser emission from the  $J = 2 - 1$  and  $J = 7 - 6$  transitions and compare them with interferometry data at  $J = 1 - 0$  and with predictions from hydrodynamic models. We conclude that the ‘clump’ model of maser emission is consistent with the observations and that a plausible scenario can be constructed for the evolution of the maser emission, both high and low frequency, from the envelope of R Aqr.

In the case of low-frequency masers, including both the  $J = 1 - 0$  and  $J = 2 - 1$  data discussed in this work, the passage of a shock-wave through the envelope both creates and destroys maser clumps. Clumps upstream of the shock are destroyed, whilst new features appear downstream of the shock, after a short time delay required for cooling, provided that post-shock conditions are suitable for the developing instability clumps to support masers.

When the shock is close to the star, the balance is in favour of destruction, but an adequate supply of clumps remains upstream to maintain the low-frequency spectra: it is important that these masers can still emit near the inter-shock background temperature of the envelope, in the range 1500–2000 K, whilst the 300-GHz masers cannot. This phase of net destruction is associated with the latter stages of envelope contraction and the early stages of expansion.

Later, the production of new clumps behind the shock far outweighs the loss of the few remaining upstream clumps and the low-frequency emission passes through a maximum near a model phase of 0.85 (optical phase  $\sim 0.4$ ).

By contrast, the high frequency ( $J = 7 - 6$ ) maser clumps are present only fairly close behind the outward propagating shock: the upstream gas is too cool to support these masers. Further cooling means that replenishment of high-frequency emitting clumps must be sustained by the shock and that the radial range over which the  $J = 7 - 6$  clumps can exist is restricted: their numbers are therefore low and as the shock weakens, the spectrum is rapidly depleted. The time range suitable for producing  $J = 7 - 6$  emitting clumps lies roughly between model phases 0.25 and 0.7.

Most maser clumps emit in several transitions simultaneously (Humphreys et al. 1996) but conditions suitable for high-frequency emission are likely to be found only near the beginning of the lifetime of a clump. Clumps which can emit at even higher frequency transitions ( $J = 8 - 7$  and above) are likely to be rarer still.

#### ACKNOWLEDGMENTS

We thank the director and staff of the James Clerk Maxwell Telescope which is operated by the Royal Observatories on behalf of the Particle Physics and Astronomy Research

Council (PPARC) of the United Kingdom, the Netherlands Organisation for Scientific Research and the National Research Council of Canada. We would also like to thank Lars Nyman for supplying the SEST data presented here. MDG acknowledges the award of a University Research Fellowship by the Royal Society; RJI and JAY acknowledge awards from PPARC. In this research, we have used, and acknowledge with thanks, data from the AAVSO International Database, based on observations submitted to the AAVSO by variable star observers worldwide.

#### REFERENCES

- Beck H.K.B., Gail H.-P., Henkel R., Sedlmayr E., 1992, *A&A*, 265, 626
- Boboltz D.A., Diamond P.J., Kemball A.J., 1997, *ApJ*, 487, L147
- Bowen G., 1988, *ApJ*, 329, 299
- Bowen G., 1989, in NATO Advanced Workshop, Numerical Modelling of Nonlinear Stellar Pulsations. Problems and Prospects. Les Arcs, France
- Cuntz M., Muchmore D.O., 1994, *ApJ*, 433, 303
- Diamond P.J., Kemball A.J., Junor W., Zensus A., Benson J., Dhawan V., 1994, *A&A*, 430, L61
- Doel R.C., Gray M.D., Humphreys E.M.L., Braithwaite M.F., Field D., 1995, *A&A*, 302, 797
- Gray M.D., Humphreys E.M.L., Field D., 1995, *ApSS*, 224, 63
- Gray M.D., Ivison R.J., Yates J.A., Humphreys E.M.L., Hall P.J., Field D., 1996, *MNRAS*, 277, L67
- Greenhill L.J., Colomer F., Moran J.M., Backer D.C., Danchi W.C., Bester M., 1995, *ApJ* 449, 365
- Humphreys E.M.L., Gray M.D., Yates J.A., Field D., Bowen G., Diamond P.J., 1996, *MNRAS*, 282, 1359
- Humphreys E.M.L., Gray M.D., Yates J.A., Field D., 1997a, *MNRAS*, 287, 663
- Humphreys E.M.L., Gray M.D., Field D., Yates J.A., Bowen G., Diamond P.J., 1997b, submitted
- Ivison R.J., Seaquist E.R., Hall P.J., 1994, *MNRAS*, 269, 218
- Ivison R.J., Seaquist E.R., Hall P.J., 1995, in Watt G.D., Williams P.M., eds, *Circumstellar matter 1994*, Kluwer, Dordrecht, p. 255
- Ivison R.J., Yates J.A., Hall P.J., 1998, *MNRAS*, in press
- Kholopov P.N. (ed.), 1985, ‘General Catalogue of Variable Stars’, 4th edition, Nauka, Moscow
- Martinez A., Bujarrabal V., Alcolea J., 1988, *A&AS*, 74, 273
- Miyoshi M., Matsumoto K., Kameno S., Takaba H., Iwata T., 1994, *Nat*, 371, 395
- Nyman L.-Å., Olofsson H., 1986, *A&A*, 158, 67
- Padman R., 1993, ‘SPECX Users’ Manual’, Cavendish Laboratory, Cambridge
- Schwarz H.E., Nyman L.-Å., Seaquist E.R., Ivison R.J., 1995, *A&A*, 303, 833
- Wirsih J., 1988, *ApJ*, 331, 463
- Woitke P., Krüger D., Sedlmayr E., 1996, *A&A*, 311, 927